JBIC Journal of Biological Inorganic Chemistry
https://doi.org/10.1007/s00775-020-01805-z

ORIGINAL PAPER

Pentacyanoferrate(II) complex of pyridine-4- and pyrazine-2-hydroxamic acid as source of HNO: investigation of anti-tubercular and vasodilation activities

Edinilton Muniz Carvalho[1,2,3] · Tercio de Freitas Paulo[1,2,3] · Alix Sournia Saquet[1] · Bruno Lopes Abbadi[4,5] · Fernanda Souza Macchi[4,5] · Cristiano Valim Bizarro[4,5] · Rafael de Morais Campos[6] · Talles Luann Abrantes Ferreira[6] · Nilberto Robson Falcão do Nascimento[6] · Luiz Gonzaga França Lopes[3,5] · Remi Chauvin[1,2] · Eduardo Henrique Silva Sousa[3,5] · Vania Bernardes-Génisson[1,2]

Received: 4 May 2020 / Accepted: 5 July 2020

Abstract

A pharmacophore design approach, based on the coordination chemistry of an intimate molecular hybrid of active metabolites of pro-drugs, known to release active species upon enzymatic oxidative activation, is devised. This is exemplified by combining two anti-mycobacterial drugs: pyrazinamide (first line) and delamanid (third line) whose active metabolites are pyrazinoic acid (PyzCOOH) and likely nitroxyl (HNO (or $NO^{\cdot}$)), respectively. Aiming to generate those active species, a hybrid compound was envisaged by coordination of pyrazine-2-hydroxamic acid (PyzCONHOH) with a $Na_3[Fe^{II}(CN)_5]$ moiety. The corresponding pentacyanoferrate(II) complex $Na_4[Fe^{II}(CN)_5(PyzCONHO^{-})]$ was synthesized and characterized by several spectroscopic techniques, cyclic voltammetry, and DFT calculations. Chemical oxidation of this complex with H_2O_2 was shown to induce the release of the metabolite PyzCOOH, without the need of the *Mycobacterium tuberculosis* (*Mtb*) pyrazinamidase enzyme (PncA). Control experiments show that both H_2O_2- and N-coordinated pyrazine Fe^{II} species are required, ruling out a direct hydrolysis of the hydroxamic acid or an alternative oxidative route through chelation of a metal center by a hydroxamic group. The release of HNO was observed using EPR spectroscopy in the presence of a spin trapping agent. The devised iron metal complex of pyrazine-2-hydroxamic acid was found inactive against an actively growing/non-resistant *Mtb* strain; however, it showed a strong dose-dependent and reversible vasodilatory activity with mostly lesser toxic effects than the reference drug sodium nitroprussiate, unveiling thus a potential indication for acute or chronic cardiovascular pathology. This is a priori a further indirect evidence of HNO release from this metal complex, standing as a possible pharmacophore model for an alternative vasodilator drug.

Keywords Blood vessel vasodilation · Hybrid pro-drug activation · Metallodrug · Pyrazinamide · Sodium nitroprusside derivative · Tuberculosis

Introduction

Tuberculosis, a millennial disease due to the infection by *Mycobacterium tuberculosis* (*Mtb*), remains today a worldwide health problem causing more than 1 million deaths annually and being responsible for latent infections in about one third of the global population [1].

Although the cure of tuberculosis can be achieved by a therapeutic regimen involving four frontline drugs, isoniazid (INH), rifampicin, ethambutol and pyrazinamide (PYZ) (Scheme 1), without treatment, tuberculosis becomes lethal. Moreover, the first-line therapy is inefficient against multi

Electronic supplementary material The online version of this article (https://doi.org/10.1007/s00775-020-01805-z) contains supplementary material, which is available to authorized users.

✉ Eduardo Henrique Silva Sousa
eduardohss@dqoi.ufc.br

✉ Vania Bernardes-Génisson
vania.bernardes-genisson@lcc-toulouse.fr

Extended author information available on the last page of the article

Published online: 29 July 2020

and extensively drug-resistant *Mtb* strains, which are of increasing importance.

Second- and third-line drugs should thus be used against these virulent *Mtb* strains. However, these drugs display numerous toxic side effects, and even for them, resistant *Mtb* strains are emerging.

Recently, a novel antitubercular drug, delamanid [2] (Scheme 2), was approved as a third-line drug of the anti-tuberculosis therapy. This molecule has two particular interests: on the one hand, only a few cases of resistance have been yet reported, and, on the other, it acts upon both dormant and replicating *Mtb* strains [3, 4]. Delamanid, a nitro-dihydro-imidazole derivative, is reported as a pro-drug and thus requires an enzymatic activation step. The active metabolite is described as being nitroxyl, i. e. HNO (protonated one-electron reduced form of nitric oxide, NO·), resulting from a reductive decomposition of the nitroimidazole group by a mycobacterial nitroreductase enzyme (Ddn) [5, 6]. However, a possible action of the NO· radical cannot be entirely ruled out. On the other hand, no organic metabolite arisen from this bio-reductive activation step was until now identified as a bacterial growth inhibitor.

It is interesting to note that while HNO/NO· may exhibit anti-tuberculosis activities, it is also known to play a very important role on other biological processes as an anti-oxidant [7], anti-angiogenic [8], and also as a vasorelaxant agent [9]. Indeed, cardiovascular diseases are among the major causes of deaths around the world, for which there is an urgent need for new therapeutic agents, including HNO and nitric oxide (NO·) donors. Sodium nitroprusside, a nitrosylpentacyanoferrate(II) complex, is the only clinically approved metal-based nitric oxide donor, which has been used in cardiovascular emergency procedures for over 50 years. In contrast, there is no HNO donor agent clinically available so far. Together these examples show that HNO

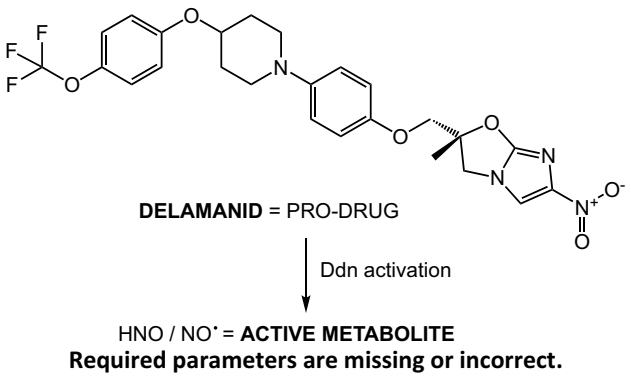

Scheme 2 Structure of the delamanid anti-tubercular pro-drug and its active metabolite(s)

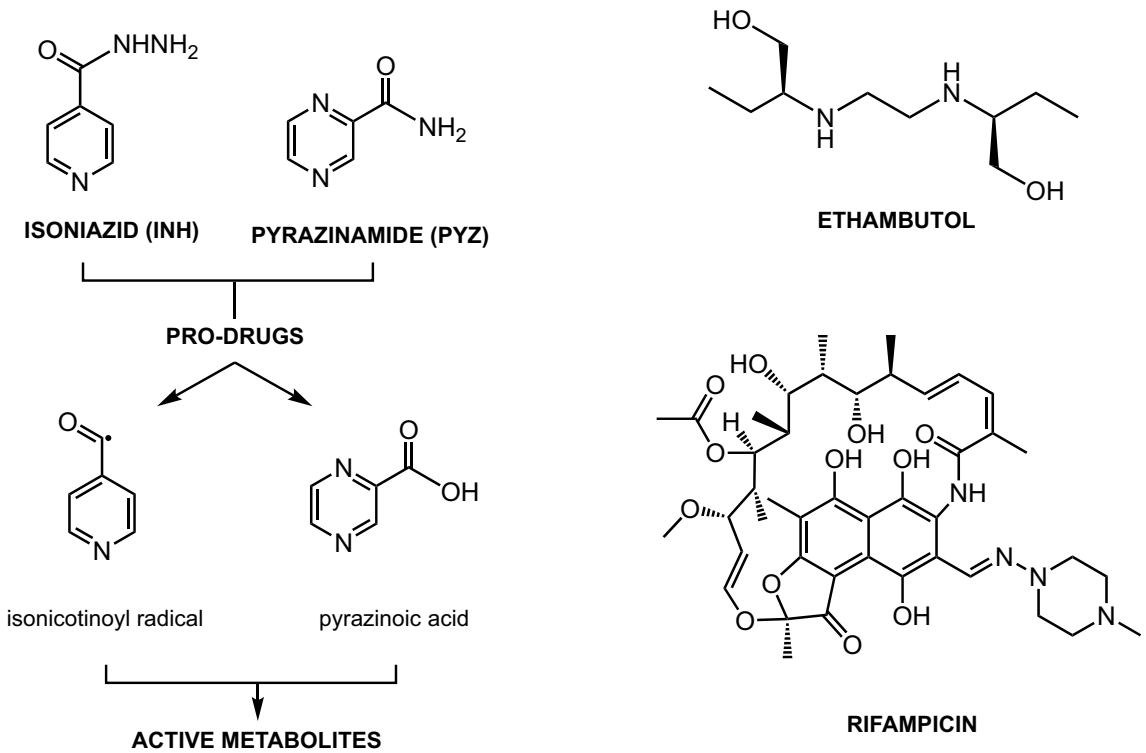

Scheme 1 First-line anti-tubercular (pro-)drugs and reactive species generated from the isoniazid and pyrazinamide pro-drugs.

donor molecules can be of great interest in the medical field as potential therapeutic agents.

Lately, some of the present authors have studied and developed a biomimetic system, as an alternative non enzyme-dependent way to activate the INH antituberculosis pro-drug (KatG = activation enzyme of INH), based on the redox reactivity of a metal complex of INH (called IQG607) in the presence of oxidizing agents such as H_2O_2 [10–12]. The anti-mycobacterial activity (in vitro $MIC_{Mtb} = 1.56$ µg/mL ~ 3.5 µM) [13], chemical stability, and absence of toxicity (selectivity index SI > 4000, $LD_{50} > 2000$ mg/kg) [14] of the $[Fe^{II}(CN)_5(INH)]^{3-}$ complex motivated us to extend this activation approach to heteroaryl hydroxamic acids used as ligands for the development of new HNO donor complexes. Thereby, to prepare HNO donors from $[Fe^{II}(CN)_5$(heteroaryl hydroxamic acid)] complexes with wide spectra of biological activities, including antituberculosis, the pyrazine-type nitrogen aryl ring was naturally first selected and used in this study. The pyrazine moiety is already present in the structure of a first-line antitubercular drug, pyrazinamide (PYZ, see Scheme 1). Pyrazinamide, like isoniazid and delamanid, is also a pro-drug and is activated by pyrazinamidase (PncA), an enzyme of *Mtb* [15, 16]. This reaction converts the pro-drug into the corresponding carboxylic acid (pyrazinoic acid = PyzCOOH) that is assigned to be the effective toxic agent for *Mtb* (Scheme 1). The sensitivity of *Mtb* to this drug is partly due to an inefficient efflux of PyzCOOH, that is found accumulated in the interior of the cell [17, 18].

Considering that the major route for PYZ resistances relies on point mutations on the PncA enzyme that is responsible for the conversion of PYZ into pyrazinoic acid [17–19], the synthesis of the $Na_3[Fe^{II}(CN)_5$(PyzCONHOH)] complex, could be judicious because the proposed complex can be considered as a hybrid source of the active metabolites of PYZ and delamanid that, under oxidative conditions, could generate, in an opportunistic way, two antitubercular agents, HNO and pyrazinoic acid. Both metabolites could be ideally released without the need of mycobacterial enzymes (overcoming resistance phenomena) and could act upon multiple targets simultaneously, reducing the chances of selection of resistant bacterial cells.

This paper mainly describes the synthesis, characterization, and chemical–biological studies of pyrazine-2-hydroxamic acid (**2**) and its pentacyanoferrate(II) complex **3** (Scheme 3). As proposed above, the ligand **2** is actually a functional hybrid of two different pharmacophores corresponding to the active metabolites of PYZ (PyzCOOH) and delamanid (HNO). After chemical activation of the prototype complex **3** (Fe(II) converted to Fe(III) upon oxidation), and independently of the functional state of the activating enzyme of *Mtb* (mutated or not), the released pharmacophores are expected to recognize different targets and act by different mechanisms, killing growing and, more particularly, non-growing *Mtb* strains (Scheme 3).

Isonicotinohydroxamic acid has also been synthesized in view of the fact that putative isonicotinic acid, formed after the activation step, can be considered as a bio-isostere of pyrazinoic acid.

Material and methods

Chemicals

Available reagents and solvents were purchased from commercial suppliers and used without further purification: methyl isonicotinate, methyl pyrazine-2-carboxylate (Alfa Aesar); hydroxylamine solution (NH_2OH, 50% in water) from Sigma-Aldrich, pyrazinoic acid, isonicotinic acid and potassium ferricyanide (III) ($K_3[Fe(CN)_6]\cdot 3H_2O$) from Sigma-Aldrich; isoniazid (INH) from ACROS

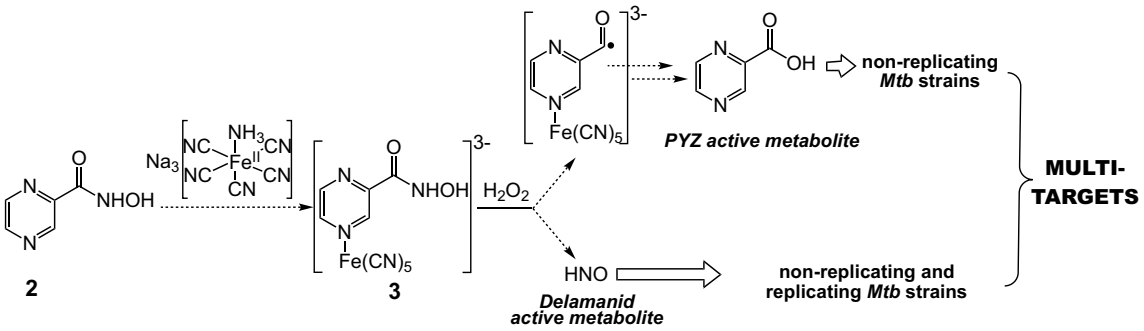

Scheme 3 Possible outcome route for oxidation of the $Na_3[Fe^{II}(CN)_5$(PyzCONHOH)] complex by H_2O_2

Organics; sodium dihydrogen phosphate (NaH_2PO_4), disodium hydrogen phosphate (Na_2HPO_4) and sodium trifluoroacetate ($NaC_2F_3O_2$) from PROLABO and Fluka; 2-(4-carboxyphenyl)-4,4,5,5-tetramethylimidazoline-1-oxyl-3-oxide potassium salt (c-PTIO) and *N-tert*-butyl-α-phenylnitrone (PBN), used as radical trapping agents, from Thermo Fisher Scientific and Alfa Aesar, respectively.

$Na_3[Fe^{II}(CN)_5(NH_3)]\cdot 3H_2O$ was prepared as previously described [20]. Methanol, ethanol, dichloromethane, and acetone were of chromatographic grade, and water used in the experiments was ultra-purified using a Milli-Q system (Millipore).

Instruments

^{1}H NMR spectra were recorded on a Bruker spectrometer at 300 and 400 MHz using D_2O and DMSO-*d*6 as solvents, with increasing chemical shifts at low field vs the tetramethylsilane ^{1}H nucleus reference derived from the deuterium lock signal of the solvent. ^{13}C NMR spectra were recorded on a Bruker spectrometer at 101 MHz using D_2O and DMSO-*d*6 as solvents, with increasing chemical shifts at low field vs the tetramethylsilane ^{13}C nucleus reference derived from the deuterium lock signal of the solvent. ^{15}N NMR spectra were recorded on a Bruker spectrometer at 50.7 MHz and external sample of CH_3NO_2 was used as the reference. Electrospray mass spectra (ESI) were obtained on a Perkin–Elmer SCIEX API 365 instrument high resolution and desorption chemical ionization (DCI) mass spectra were acquired on a Finnigan TQS 7000 spectrometer. Infrared spectra were obtained using a Perkin–Elmer Spectrum One spectrometer. UV–Vis spectra were recorded on a Perkin–Elmer UV/Vis/NIR Spectrometer—Lambda 950. Normal Raman (NR) spectra of the samples were acquired by means of an Xplora (Horiba) microspectrometer: the excitation radiation was the 785 nm line and the laser beam was focused on the sample by a × 50 long distance objective. Elemental analyses were obtained using a PERKIN ELMER 2400 series II instrument. Electrochemical measurements were performed using a BAS Epsilon E2 818 potentiostat/galvanostat system within a conventional three-electrode cell. Vitreous carbon, platinum, and calomel electrodes were used as working, auxiliary and reference electrodes, respectively. Voltammograms were recorded in phosphate buffer solution (PBS) 0.1 M, pH 7.4. Electron paramagnetic resonance (EPR, or electron spin resonance = ESR) spectra were recorded at room temperature (ca. 291 K) on a Bruker Elexsys-II E500 (X-Band) spectrometer using a modulation amplitude of 0.5 G, a microwave power of 5.15 mW, with an attenuation of 16 dB with repeated number of 2 scans. The samples were transferred into a capillary (Hirschmann, Duran, Ringcaps, 50 µL), which was then placed inside a larger quartz tube enabling the sample to be accurately positioned inside the resonator. All samples were prepared as 40 mM solutions in phosphate buffer pH 7.4, at 25 °C, by mixing suitable amounts of the studied compound and spin trap (cPTIO or PBN). The reactions were initiated by the addition of the H_2O_2 and the spectra immediately recorded.

Synthetic procedures

General procedure for hydroxamic synthesis

To a solution of methyl heteroaryl-carboxylate derivative (3.62 mmol) in methanol (10 mL) at room temperature and under stirring, 3.9 mL of hydroxylamine 50% (65.2 mmol) was slowly added. The solution was stirred for 72 h. The solvent was evaporated under vacuum and the solid was resuspended in dichloromethane, filtered, and thus washed from traces of pyrazine-2-carboxylate. Then, the solid was resuspended in water (4 mL) to remove traces of hydroxylamine: the pyrazine-2-hydroxamic acid being poorly soluble in water, the mixture was cooled down in an ice bath for 3 h to assist the product precipitation. Then, the solid was filtered, washed with cold acetone, and dried under vacuum.

Pyrazine-2-hydroxamic acid (2)

Yield = 85% (0.43 g), white solid. ^{1}H NMR (400 MHz, DMSO-d_6) δ (ppm): 11.62 (s, 1H), 9.28 (s, 1H), 9.12 (d, J = 1.5 Hz, 1H), 8.84 (d, J = 2.5 Hz, 1H), 8.68 (dd, J = 2.5, 1.5 Hz, 1H). ^{13}C NMR (101 MHz, DMSO-d_6) δ (ppm): 160.65 (C=O), 147.75 (CH), 145.52 (Cq), 143.85 (CH), 143.67 (CH). ^{15}N NMR (50.7 MHz, D_2O) δ (ppm): 319.30 (N_1), 323.36 (N_4). IR symmetric stretching (ν_s), anti-symmetric stretching (ν_{as}), symmetric bending (δ_s) and twisting (τ) (cm^{-1}): 3212 (ν_s O–H), 3061 (ν_s N–H), 2823 (ν_s C–H), 1662 (ν_s C=O), 1585 – 1524 ν C=N, ν_s C=C), 1417 (δ_s N–H), 1386 (δ_s C–H), 1023 (ν_{as} C=N), 916 (τ C–H). UV–Vis (H_2O) ν_{max}/nm (ν/M^{-1} cm^{-1}) = 211 (8169), 272 (7248), 312 (876). MS (DCI/CH_4) *m/z*: 140.04 [M + H^+], 124.05 [(M + H^+)-16]. HRMS (DCI/CH_4) *m/z*: for {($C_5H_5N_3O_2$) + H^+} calcd.: 140.0460 found: 140.0464. Elemental analysis calcd. for $C_5H_5N_3O_2$: C, 43.17; H, 3.62; N, 30.21. Found: C, 42.91; H, 3.51; N, 29.81. TLC (dichloromethane/methanol 90:10) R_f = 0.42. M.p. = 165 °C. Electrochemistry in 0.1 M phosphate buffer, pH 7.4, E_{pa} = 0.684 and 1.119 V vs NHE.

Pyridine-4-hydroxamic acid (5)

Yield = 98% (0.49 g), white solid. ^{1}H NMR (300 MHz, DMSO-d_6) δ (ppm): 11.50 (s, 1H), 9.32 (s, 1H), 8.70 (d, J = 6.1 Hz, 2H), 7.67 (d, J = 6.1 Hz, 2H). ^{13}C NMR (101 MHz, DMSO-d_6) δ (ppm): 162.48 (Cq), 150.68 (CH), 140.31 (Cq), 121.40 (CH). IR symmetric stretching (ν_s), anti-symmetric stretching (ν_{as}), symmetric bending (δ_s) and twisting (τ) (cm^{-1}) ν_{max} (cm^{-1}): 3324 (ν_s O–H), 3132 (ν_s N–H), 1640 (ν_s C=O), 1540–1520 (ν_s C=N, ν_s C=C), 1410 (δ_s N–H), 1316 (δ_s C–H), 1025 (ν_{as} C=N), 908 (τ C–H). UV–Vis (H_2O) λ_{max}/nm (ε/M^{-1} cm^{-1}) = 235 (3760), 260 (3710). HRMS (DCI/CH_4): for {($C_6H_6N_2O_2$) + H^+} calcd.: 139.0508 found: 139.0515. Elemental analysis calcd. for $C_6H_6N_2O_2$: C, 52.17; H, 4.38; N, 20.28. Found: C, 52.12; H, 4.21; N, 20.25. TLC (dichloromethane/methanol 90:10) R_f = 0.24. M.p = 154 °C. Electrochemistry in 0.1 M phosphate buffer, pH 7.4, E_{pa} = 0.767 and 1.207 V vs NHE.

General procedure for preparation of $Na_4[Fe^{II}(CN)_5$(HeteroarylCONHO$^-$)]compounds

To a solution of $Na_3[Fe^{II}(CN)_5(NH_3)]\cdot 3H_2O$ (0.150 g, 0.46 mmol, 1 equiv.) in water (3 mL), it was slowly added a solution of the ligand (pyrazine-2-hydroxamic acid, 0.077 g, 0.55 mmol, 1.2 equiv. or pyridine-4-hydroxamic acid, 0.076 g, 0.55 mmol, 1.2 equiv.) in water (2 mL). The mixture was stirred at room temperature, under argon atmosphere and protected from light for 3 h. Then 150 mL of a cold solution of ethanol containing an excess of sodium iodide (30 equiv.) was added dropwise. The resulting precipitate was kept overnight at −20 °C before it was collected by filtration, washed with cold ethanol, and dried in a vacuum desiccator. CAUTION: since these complexes are moderately light and oxygen sensitive, they must be stored in a vacuum desiccator protected from light to extend their lifetime.

$Na_4[Fe^{II}(CN)_5$(PyzCONHO$^-$)] ($Na_4$3) (PyzCONHO$^-$ = pyrazine-2-hydroxamate)

Yield = 87% (0.180 g), orange solid. ^{1}H NMR (400 MHz, D_2O) δ (ppm): 9.46 (s, 1H), 9.18 (d, J = 3.3 Hz, 1H), 8.27 (d, J = 3.2 Hz, 1H). ^{13}C NMR (101 MHz, D_2O) δ (ppm): 178.69 (CN_{eq}), 173.75 (CN_{ax}), 160.69 (C=O), 153.77 (CH), 150.66 (CH), 145.50 (Cq), 142.33 (CH). ^{15}N NMR (50.7 MHz, D_2O) δ (ppm): 301.10 (N_4), 308.56 (N_1). IR symmetric stretching (ν_s), antisymmetric stretching (ν_{as}), symmetric bending (δ_s), antisymmetric bending (δ_{as}) and wagging (π) (cm^{-1}): 3418 (ν_s N–H), 3452–3250 (ν_s C–H), 2053 (ν_s C≡N), 1609 (ν_s C=O), 1577 (ν_s C=N, C=C), 1391—1173 (δ_s C–H), 1033 (τ C–H). 908 (δ_{as} C–H), 854 and 753 (π C–H), 652 (ν_s C=N). UV–Vis (H_2O) λ_{max}/nm (ε/M^{-1} cm^{-1}) = 216 (18,820), 270 (6228), 486 (3638). Elemental analysis calcd. for $C_{10}H_4FeN_8O_2Na_4\cdot 3H_2O$: C, 25.55; H, 2.14; N, 23.84. Found: C, 25.93; H, 2.16; N, 23.94. Electrochemistry in phosphate buffer (0.1 M, pH 7.4): E_{pa} = 0.722 and 1.091 V vs NHE.

$Na_4[Fe^{II}(CN)_5$(PyCONHO$^-$)] ($Na_4$6) (PyCONHO$^-$ = pyridine-4-hydroxamate)

Yield = 79% (0.173 g), yellow solid. ^{1}H NMR (400 MHz, D_2O) δ (ppm): 9.05 (d, J = 4.96, 2H), 7.39 (d, J = 4.76, 2H). ^{13}C NMR (101 MHz, D_2O) δ (ppm): 180.64 (CN_{eq}), 176.39 (CN_{ax}), 164.02 (Cq), 157.34 (CH), 141.63 (Cq), 120.52 (CH). IR symmetric stretching (ν_s), antisymmetric stretching (ν_{as}), symmetric bending (δ_s), antisymmetric bending (δ_{as}), wagging (π), rocking (ρ) and twisting (τ) (cm^{-1}): 3483 (ν_s N–H), 3382–3047 (ν_s C–H), 2052 (ν_s C≡N), 1647 (ν_s C=O), 1546 (ν_s C=N, C=C), 1492—1414 (δ_s C–H), 1313 (π C–H), 1227 (τ C–H), 1165 (ν_s C–C). 908 (δ_{as} C–H), 846 (π C–H), 698 (π N–H). UV–vis (H_2O) λ_{max}/nm (ε/M^{-1} cm^{-1}) = 233 (14,400), 266 (5123), 439 (4052). Elemental analysis calcd. for $C_{11}H_5FeN_7O_2Na_4\cdot 3.5H_2O$: C, 27.64; H, 2.53; N, 20.51. Found: C, 27.66; H, 2.21; N, 20.76. Electrochemistry in 0.1 M phosphate buffer (pH 7.4): E_{pa} = 0.551 and 1.099 V vs NHE.

Computational details

All calculations were carried out using the density functional theory (DFT) with the B3LYP [21–23] functional as implemented in the Gaussian 09 program package, Revision D.01 (Gaussian Inc., Wallingford, CT) [24]. The 6-311++G(d,p) basis set was used for non-metal atoms, while the LANL2DZ relativistic effective core potential basis set was used for Fe atoms. Vibrational frequency analyses were carried out to confirm convergence to a minimum energy geometry by the absence of imaginary frequencies. A scaling factor of 0.9679 for the calculated harmonic vibrational wavenumbers considering the 6-311++G(d,p) basis set and the B3LYP functional. The vertical excitation energies were determined by the time-dependent density functional theory protocol (TD-DFT) using the B3LYP functional and mixed basis sets mentioned above. The polarizable continuum model (PCM) [25] was used in the case of vertical excitation energies to take into account the solvent effect, where the dielectric constant of water was considered. The FTIR, UV–Vis spectra were extracted from output files, while Raman spectra were calculated with the GaussSum 3.0 program [26]. This program was used to calculate the Raman intensity considering an exciting radiation of 785 nm.

Antimycobacterial activity

In vitro activity of the compounds **2**, **3**, **5** and **6** was evaluated against the *Mycobacterium tuberculosis* H37Rv ATCC 27294 reference strain (American Type Culture Collection, Rockville, Md.), by performing minimum inhibitory concentration assays (MIC), as described elsewhere [27]. This strain was grown up to mid-log phase (OD_{600} 0.8–1.0) in Middlebrook 7H9 broth (Difco™), supplemented with 10% ADC (albumin, dextrose and catalase—BD BBL™) and 0.05% Tween 80 (Sigma-Aldrich), with agitation (100 rpm), at 37 °C. Following that, a mycobacterial suspension was prepared using sterile glass beads (4 mm), which was aliquoted and stored at -80 °C until use. Compounds were first solubilized in ultrapure water (4 mg/mL) and diluted in 7H9 broth (200 µg/mL). Serial twofold dilutions (100 µL) of each compound were performed directly in 96-well plates in 7H9 broth, giving a concentration range of 100–0.2 µg/mL. An aliquot of mycobacterial suspension was thawed and diluted in 7H9 broth to a theoretical OD of 0.006, which was added to each well (100 µL). Compound and culture-free wells were used as positive and negative growth controls, respectively. Isoniazid (INH, ACROS Organics) was used as an anti-TB drug reference. Plates were sealed with Parafilm M® and incubated inside plastic bags in a bacteriological incubator (37 °C, 5% CO_2) for 7 days, before the addition of 60 µL of 0.01% (w/v) resazurin (Sigma-Aldrich) solution to each well. Minimum inhibitory concentration (MIC) was considered as the lowest compound concentration that prevented a color conversion from blue (no growth) to pink (growth). MIC values reported for each compound were the most frequently occurring value observed among three independent assays. INH was used as a positive control of MIC assays.

Vasodilation assay

Rats were sacrificed by overdose of sodium thiopental and the thoracic aorta was carefully removed and cut into rings of about 5 mm in length. The aortic rings were mounted in a 5 mL organ bath containing Krebs–Henseleit medium with the following composition: 120 mM NaCl, 4.7 mM KCl, 1.8 mM $CaCl_2$, 1.43 mM $MgCl_2$, 25.0 mM $NaHCO_3$, 1.17 mM KH_2PO_4, glucose and maintained at 37 °C. The rings were attached to a force transducer (TRI202P, Panlab, Barcelona, Spain) coupled to a Powerlab data acquisition systema (ADInstruments, Sydney, Australia) and data were recorded and analyzed using the Labchart 7.0 software. After equilibration, the rings were pre-contracted with 1 µM phenylephrine (PE), and once a stable plateau was achieved, cumulative concentration–response curves were constructed using the ligand **2** and **5** and the metal complexes **3** and **6** in a concentration range from 0.1 nM to 100 µM. Sodium nitroprusside (SNP, $Na_2[Fe(CN)_5(NO)]$) was used as positive control. This assay was performed using seven independent measurements prepared with different animals for statistical analysis. All procedures were performed according to the ethics committee of State University of Ceará number 2897836/15.

Systemic hemodynamics

Male WistarKyoto (WKY) or spontaneously hypertesive rats (SHR) (250–300 g) were anesthetized with sodium pentobarbital (50 mg/kg) and a polyethylene catheter (PE 240) was inserted into the trachea to help with spontaneous breathing. The left femoral artery was isolated and canulated with a polyethylene catheter (PE 10) and this catheter was coupled to a pressure transducer (MLT844, ADInstruments, Sydney, Australia) for continuous recording of blood pressure by means of a data acquisition system (Powerlab, ADInstruments) and a Labchart 7.0 software. The right carotid artery was canulated with a microtip pressure–volume catheter (SPR-869, Millar Instruments; Houston, TX) and this catheter was inserted into the left ventricle for continuous measurement of cardiac parameters such as cardiac output.

Results and discussion

Synthesis

The ligand moiety, pyrazine-2-hydroxamic acid (**2**) (PyzCONHOH) [28, 29], of the targeted hybrid complex **3**, was directly prepared from methyl pyrazinoate (**1**) in NH_2OH solution with 85% yield (Scheme 4) and fully characterized. Then, the coordination of **2** with $Na_3[Fe(CN)_5NH_3]$ was carried out in aqueous medium to afford Na_4**3** in 87% yield (Scheme 4). This compound was analyzed by $^{1}H/^{13}C/^{15}N$ NMR, IR, UV–Vis and Raman spectroscopy, along with cyclic voltammetry, elemental analysis and DFT calculations. Attempts to obtain crystals of the complex Na_4**3** for X-ray diffraction analysis were unsuccessful. Additionally, procedures to exchange the sodium cations by other more crystallogenic/solubilizing cations (e.g. PPN^+, NEt_4^+) also failed. (Protocol a: to a solution of salt (PPN^+ or NEt_4^+) in ethyl acetate, the iron complex was added. The mixture was stirred overnight in the shadow. The solution was filtered to remove the unsolubilized complex. The filtered solution was rotoevaporated and the crude product was characterized by ^{1}H-NMR. Protocol b: an aqueous solution containing the iron complex was added to a solution of salt cation (PPN^+ or NEt_4^+) in ethyl acetate. This mixture was stirred overnight in the shadow. Then the organic and aqueous phases were separated. The organic phase was rotoevaporated and the solid obtained was characterized by ^{1}H-NMR. No signal corresponding

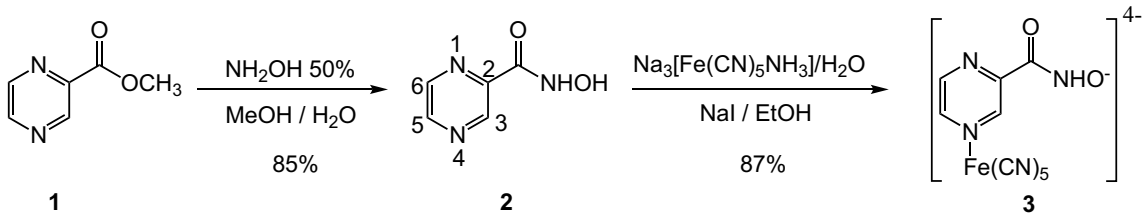

Scheme 4 Synthesis of the pentacyanoferrate(II) complex of pyrazine-2-hydroxamate from methyl pyrazine-2-carboxylate

to the complex framework was observed, just signals of the cation PPN^+ or NEt_4^+. The aqueous solution was also analyzed by ^{1}H-NMR; however, no characteristic signal of these salts was identified).

The pentacyanoferrate(II) complexes of pyridine-4-hydroxamic acid (PyCONHOH) and sodium pyrazine-2-carboxylate (PyzCOONa) were both synthesized for the purpose of comparison and for control experiments, respectively. Treatment of methyl isonicotinate **4** with hydroxylamine originated the corresponding hydroxamic acid **5** [30], which was converted to the metal complex Na_4**6,** using the same protocol employed for the preparation of **3** (Scheme 5). Likewise, deprotonation of pyrazinoic acid **7** led to sodium pyrazinoate **8**, which was then coordinated to the $Fe^{II}(CN)_5$ moiety with 64% yield in the complex **9** (see Supporting Information).

In all cases, the coordination to the diamagnetic Fe(II) center was shown to take place only at the less hindered N atom of the heteroaromatic ring as evidenced by spectroscopic analysis (see Sect. 3.2).

Characterizations

NMR spectroscopy

The ^{1}H NMR spectrum of **3** shows the aromatic protons in the vicinal positions from the *N*-$Fe(CN)_5^{3-}$ fragment (H3 *s*, 9.46 and H5 *d*, 9.18 ppm) are both shifted to low field as compared to those of the free protonated ligand **2** (PyzCONHOH: *s*, 9.11 and *d*, 8.80 ppm). On the other hand, the distal aromatic proton H6 of **3** is shifted up-field (8.27 ppm) with respect to the corresponding proton in the protonated free ligand **2** (8.68 ppm). The same trend was observed in the ^{13}C NMR spectra for the corresponding aromatic ^{13}CH nuclei. The 2D ^{1}H-^{15}N HMQC NMR spectrum of **3** unambiguously shows that coordination of **2** occurs selectively at the N-4 position of the pyrazine ring (Figure S1). As observed for the $[Fe(CN)_5(INH)]^{3-}$ complex, [31] the ^{15}N1 and ^{15}N4 signals of **2** at 319.30 and 323.36 ppm are, respectively, both shifted up-field to 308.56 and 301.11 ppm, for the complex. The more pronounced shifting undergone by N4 indicates

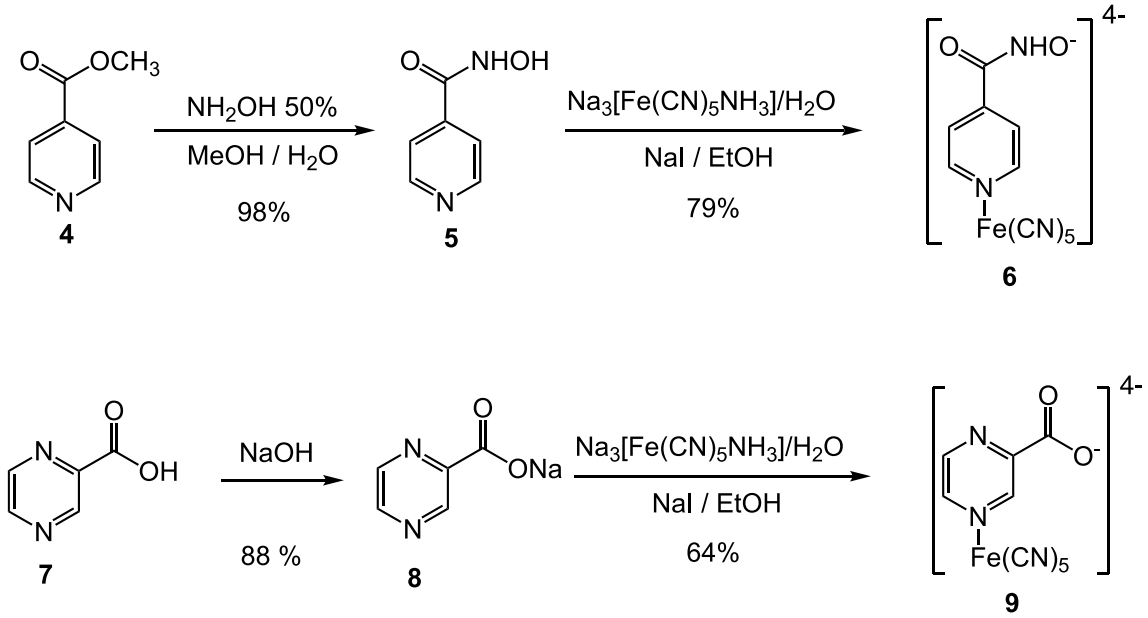

Scheme 5 Synthesis of pentacyanoferrate(II) complexes of pyridine-4-hydroxamic acid and sodium pyrazine-2-carboxylate

that the coordination of $Fe(CN)_5$ moiety occurs at this center. The high resolution of the NMR spectra of **3**, without signal broadening vs the spectra of **2**, provides a strong evidence that the iron atom of **3** is indeed in a low-spin + 2 oxidation state (Figure S1).

The cyanide ligands of **3** are revealed by two ^{13}C NMR signals at 178.7 and 173.8 ppm, characteristic of *sp* ^{13}CN nuclei in equatorial and axial positions vs the Fe–N axis. These results are consistent with those previously obtained for the pyrazine hydrazide complex $Na_3[Fe(CN)_5(PyzCONHNH_2)]$ [32].

Vibrational spectroscopy

The cyanide ligands were also characterized by infrared (IR) and Raman spectroscopy, where two bands in the range 2050–2100 cm^{-1} are assigned to the FeC≡N stretching frequencies ν(C≡N) [33]. The most relevant infrared and Raman vibration modes and wavenumbers can be found in the Supporting information (Table S1).

Unexpectedly, the experimental normal Raman spectrum of **3** in the solid state (Fig. 1) was indeed much more compatible with the corresponding DFT-simulated spectrum, than with the DFT-simulated spectrum of the O-protonated form (**3**H^+, Scheme 4). The O-deprotonated form of the ligand **2** in the tetraanionic complex **3** was also supported by elemental analysis (see experimental section). IR data reveal that the C=O band at 1662 cm^{-1} in the protonated free ligand **2** is shifted to *ca.* 1580 cm^{-1} in the complex **3**, in agreement with the anionic hydroxamate form of **2** in **3** (Scheme 4). The formation of **3** is a consequence of the basic medium (pH >> 9) used for the preparation of this complex.

The pK_a value of **3** in water solution, determined by a titrimetric method using 0.025 M HCl, is indeed as low as 8.5.

Cyclic voltammetry

Cyclic voltammograms of the ligand **2** and complex **3** in a phosphate buffer solution (0.1 M, pH 7.4) were recorded using a glassy carbon working electrode (Figure S2). For the free ligand **2**, two oxidative waves are observed at 0.68 V and 1.12 V vs NHE as irreversible electrochemical processes. In the cyclic voltammogram of the complex **3**H^+ (Figure S2 red line), the oxidation wave is observed in the potential range of 0.50–0.90 V vs NHE. This wave can be attributed to two processes corresponding to the local oxidation of the $Fe^{II} -> Fe^{III}$ and coordinated ligand. Additionally, a second irreversible electrochemical process is observed at 1.091 V vs NHE and assigned to the second ligand oxidation. The oxidation of the organic moiety likely initiates via an intramolecular process involving the formation of a Fe(III) center, although an intermolecular reaction cannot be strictly ruled out. Furthermore, there are kinetic evidences of an intramolecular electron transfer during the chemical oxidation of the $[Fe(CN)_5(INH)]^{3-}$ complex (IQG607), a process which might be similar in the chemical oxidation of **3**H^+ [10a]. In the cathodic scanning, only one wave at 0.54 V vs NHE is observed and attributed to the $Fe^{III} -> Fe^{II}$ reduction process.

UV–Vis absorption spectroscopy

The electronic spectra of the protonated free ligand **2** and complex **3**H^+ were recorded in slightly acidic aqueous

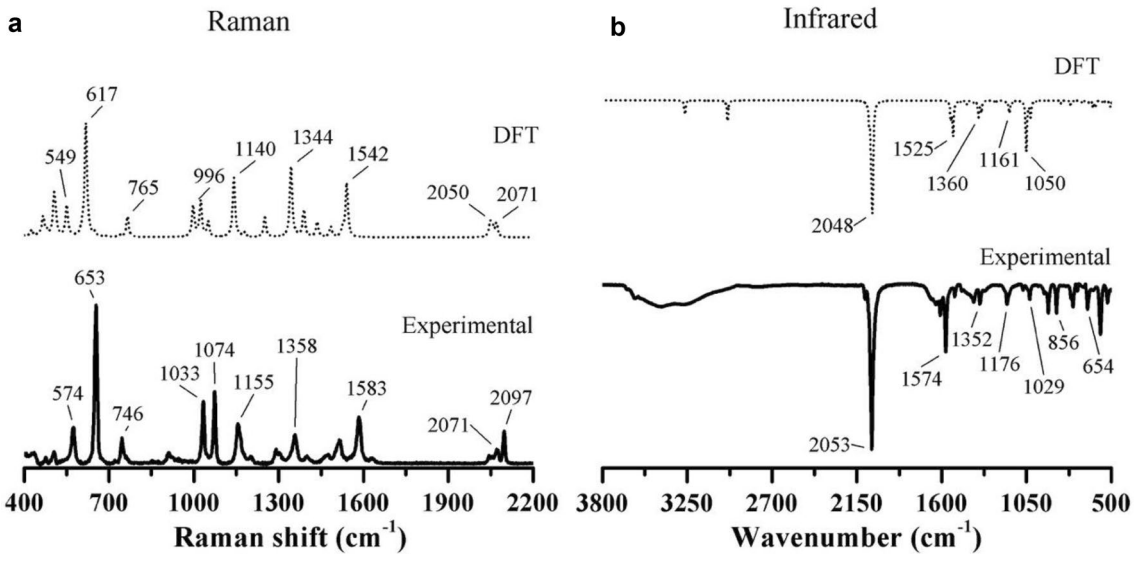

Fig. 1 Experimental normal Raman (**a**) and IR (**b**) spectra of the complex **3** under tetraanionic form, $Na_4[Fe(CN)_5L]$, L = $PyzCONHO^-$ (plain line), in the solid state, and DFT-simulated spectra for $[Fe(CN)_5L]^{4-}$ (dotted line)

solution (pH = 6.8). The free ligand **2** exhibits two main bands at 211 and 272 nm, and a shoulder at 312 nm, while the complex $\mathbf{3}H^+$ exhibits three main electronic transitions with absorption maxima at 216, 270, and 486 nm (Figure S3). The two first ones are consistent with bands relative to the ligand moiety, while the last band is characteristic of a metal-to-ligand charge transfer transition (MLCT). This type of transition occurs from an electron-rich Fe center to π-accepting ligands, which is in agreement with the + 2 oxidation state of the iron center. TD-DFT calculations further validate the character of these transitions (see Supporting information, Table S2 and Figure S4).

Chemical oxidation of the Fe(II) complex under physiological pH conditions and characterization of drug metabolites active against *Mtb*

As argued earlier, the complex $Na_4\mathbf{3}$ has been devised as a precursor of the anti-*Mtb* metabolites of pyrazinamide and delamanid, i.e. pyrazinoic acid (PyzCOOH) and nitroxyl (HNO/NO•), respectively. The search for evidences of the formation of the later organic and inorganic products upon chemical oxidation with H_2O_2 is addressed below:

Formation of PyzCOOH upon oxidation of 3

Chemical oxidation of **3** or its protonated form $\mathbf{3}H^+$ by action of H_2O_2 in a phosphate buffer solution (40 mM, pH = 7.4) can be considered as a mimic of the biological activation of PYZ by the pyrazinamidase (PncA) enzyme, which is often found mutated in PYZ-resistant *Mtb* strains. In these conditions, oxidation of **3** under its major hydroxamic acid form $\mathbf{3}H^+$ and the release of $PyzCOO^-$, without assistance of PncA, was thus investigated by UV–vis and ^{1}H NMR spectroscopy.

Before addition of H_2O_2, the trianionic complex $\mathbf{3}H^+$ (buffer solution of **3** at pH = 7.4) showed an absorption band with a maximum at 489 nm, characteristic of the MLCT transition as previously discussed. This band disappeared almost completely within 2 h (Fig. 2, red line) after addition of H_2O_2, indicating modification of the metal moiety. This result supports the hypothesis that this complex is activated by H_2O_2 via $Fe^{II} -> Fe^{III}$ oxidation (Fig. 2).

^{1}H NMR analysis of **3** in deuterated buffer solution and in the presence of 2.5 equivalents of H_2O_2, after 52 h, revealed that the signals relative to the aromatic protons of the trianionic complex $\mathbf{3}H^+$ had completely disappeared, while new signals corresponding to free pyrazine carboxylate (**8**) were observed. This was evidenced by a perfect matching of the new aromatic ^{1}H NMR signals (Fig. 3, spectrum C) with those of an authentic sample of sodium pyrazinoate (**8**) (Fig. 3, spectrum E). Remarkably, after oxidative activation, the organic metabolite **8** was found to be spontaneously released from the metal center, while only very little ligand remains coordinated to the $Fe^{II}(CN)_5^{3-}$ unit (Fig. 3, spectrum C and D)

It is worth noting that the free hydroxamic acid **2** in the presence of H_2O_2 is unable to produce pyrazinoic acid even after 52 h. In addition, in the presence of $Na_3[Fe^{III}(CN)_6]$ (2.5 equiv.), the hydroxamic group of **2** is only very slowly

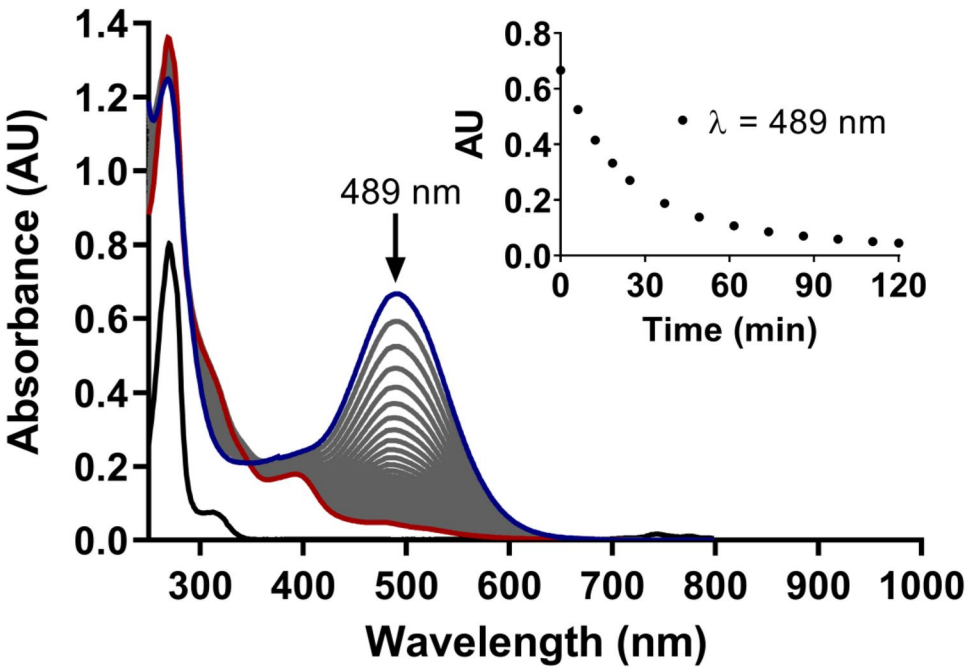

Fig. 2 UV–Vis monitoring of the reaction of **3** under the protonated main form $\mathbf{3}H^+$ (171 µM) with H_2O_2 (427.5 µM) in phosphate buffer solution, 40 mM, pH 7.4, 22 °C. Reaction at $t = 0$ min, before addition of H_2O_2, (blue line), and after 2 h (red line). The black curve corresponds to a solution of sodium 2-pyrazinoate (110 µM). Inset shows the kinetic curve based on changes at 489 nm

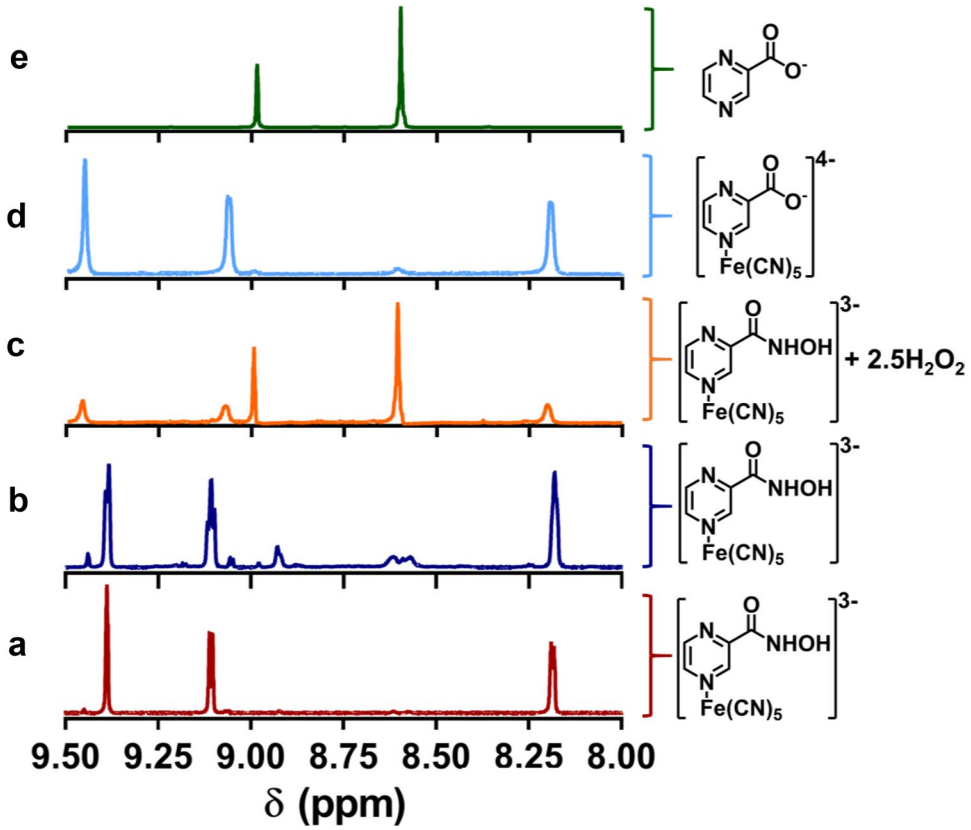

Fig. 3. ^{1}H-NMR spectra at 400 MHz: of the complex **3** under its protonated form $\mathbf{3H^{+}}$ (20 mM) at 0 h (**a**) and at 52 h (**b**) without addition of H_2O_2, at 52 h after reaction of $\mathbf{3H^{+}}$ with H_2O_2 (50 mM) (**c**), and of authentic samples of the complex **9** (20 mM) (**d**) and pyrazinoate salt (**8**) (20 mM) (**e**). Solutions in 40 mM phosphate buffer, pH 7.4, at 25 °C

and partially oxidized, and converted to the corresponding carboxylic acid PyzCOOH (even after 64 h), after hydrolysis of the putative dimer *N,O*-dipyrazinoylhydroxylamine (PyzC(O)NHOC(O)Pyz) formed as intermediate [34]. The latter intermediate has never been observed for the ligand of **3** in oxidative conditions. All together, these results show that both H_2O_2 and the N-coordinated Fe^{II} unit are needed for oxidative activation of the hydroxamic moiety, ruling out a random mechanism passing through a direct hydrolysis of the hydroxamic acid function ($PyzCONHOH + H_2O \rightarrow PyzCOOH + NH_2OH$) or an alternative activation route where the hydroxamic acid group would coordinate metal ions occasionally present in buffer solutions.

Formation of HNO/NO upon oxidation of 3

The inorganic metabolite of delamanid, i.e. the weak acid nitroxyl (HNO) or radical nitric oxide (NO), was targeted. Discrimination between these possible products was envisaged by EPR spectroscopy in the presence of the 2-(4-carboxyphenyl)-4,4,5,5-tetramethylimidazoline-1-oxyl-3-oxide potassium salt (cPTIO). This compound is a water-soluble nitronyl-nitroxide known to be readily reduced by NO, of which it is a specific scavenging agent, to give the corresponding cPTI nitroxide and the NO_2 radical (Scheme S1). This species (cPTI) presents characteristic EPR signatures different from the quintuplet signal of cPTIO (a septet for cPTI) [34]. cPTIO also reacts with HNO, by which it is reduced to the EPR-silent nitronyl-hydroxylamine, while releasing the NO radical (Scheme S1) [35, 36].

The first control of cPTIO with the free hydroxamic acid **2** or complex **3** showed that the EPR signal of cPTIO was not altered, even after 15 min (Fig. 4b, d). The same stability of cPTIO was observed in the presence of H_2O_2 and with the mixture of $FeCl_2 + H_2O_2$, a Fenton-reaction system generating hydroxyl radicals (Fig. 4c, e). Moreover, EPR monitoring did not show any evidence of reaction of cPTIO with $Na_3[Fe^{III}(CN)_6]$ (Fig. 4f). However, a net decrease of the cPTIO EPR signal was observed upon treatment of the Fe^{II} complex **3** with H_2O_2, indicating neutralization of the nitroxide radical, which would be a priori due to the release of HNO (Fig. 4a).

Our previous studies on the activation of $Na_3[Fe(CN)_5(INH)]$ (IQG607) complex in the presence of H_2O_2 gave evidences (by EPR spectroscopy) for the formation of the isonicotinoyl radical as an intermediate towards isonicotinoic acid [31, 37]. On this basis, it was decided to check whether the hydroxamate complex **3** or its acidic form $\mathbf{3H^{+}}$ could also generate pyrazinoic acid via a transient radical intermediate what could be an indirect evidence for the formation of NO·. By employing the same methodology used before for the investigation of the INH

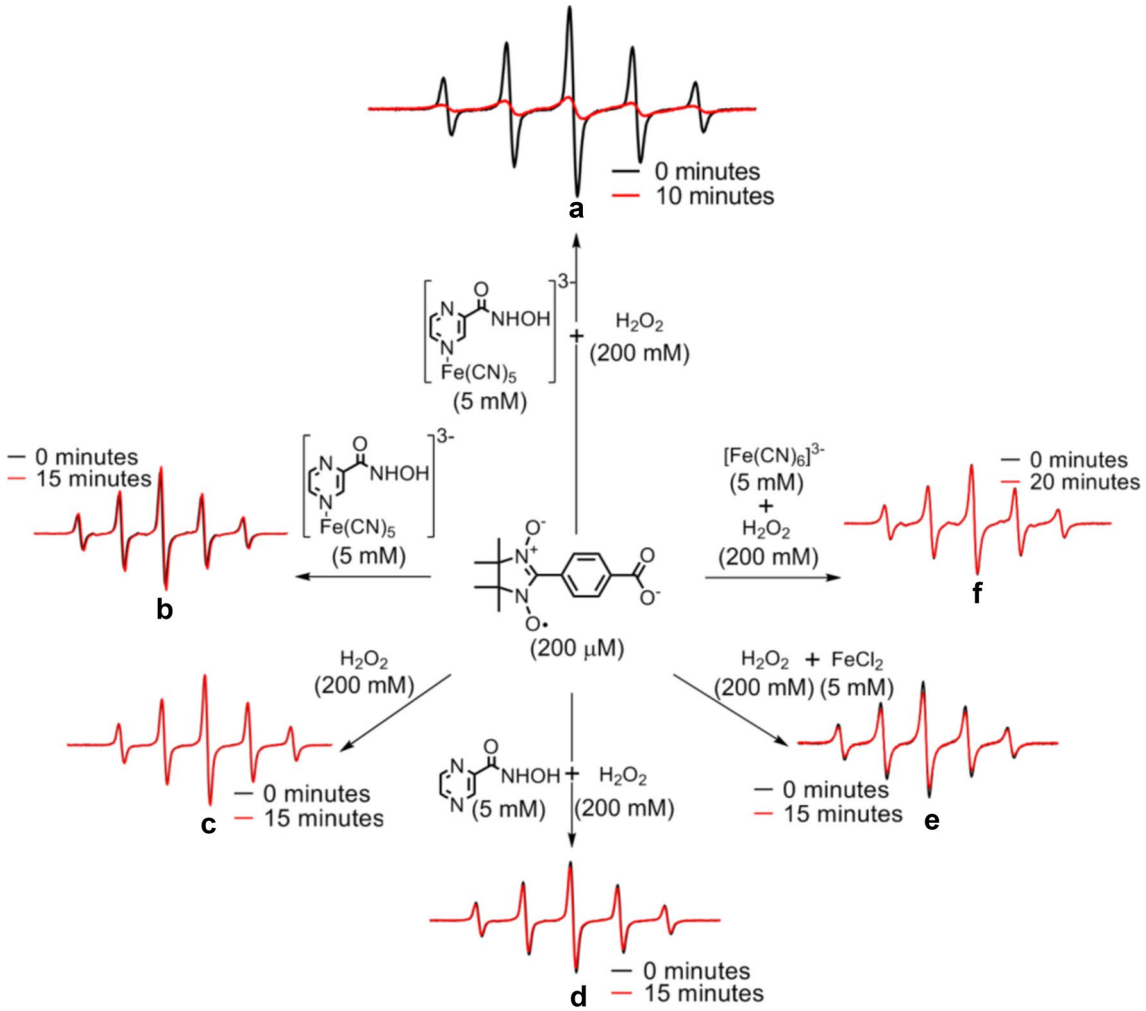

Fig. 4 **a** EPR signal of the cPTIO radical in the presence of the complex **3** under its protonated form $\mathbf{3H^+}$ and H_2O_2 (t_0 = black line and t_{10min} = red line) in phosphate buffer solution, 40 mM, pH 7.4. **b** Control of the stability of the cPTIO EPR signal in the presence of $Na_3Fe(CN)_5$-PyzCONHOH] (t_0 = black line and t_{15min} = red line). **c** Control of the stability of the cPTIO EPR signal in the presence of H_2O_2 (t_0 = black line and t_{15min} = red line). **d** Control of the stability of the cPTIO EPR signal in the presence of the ligand PyzCONHOH and H_2O_2 (t_0 = black line and t_{20min} = red line). **e** Control of the stability of the cPTIO EPR signal in Fenton reaction conditions [$FeCl_2$ (5 mM) and H_2O_2 (200 mM)] (t_0 = black line and t_{15min} = red line). **f** Control of the stability of the cPTIO EPR signal in the presence of $[Fe(CN)_6]^{3-}$ and H_2O_2 (t_0 = black line and t_{20min} = red line)

complex, EPR spectra were recorded using *N-tert*-butyl-α-phenylnitrone (PBN) as the spin trapping agent (Scheme S1B). In contrast to the parent iron complexes of isoniazid and of pyrazinoic acid hydrazide [30], $Na_3[Fe(CN)_5(INH)]$ and $Na_3[Fe(CN)_5(PyzCONHNH_2)]$, respectively, no radical could be trapped upon treatment of the pyrazine and even of the pyridine hydroxamic acid complexes (**3** and **6**, respectively), with H_2O_2 (Schemes 4 and 5).

To explain the latter results, two hypotheses can be proposed. In the case of the hydroxamic acid complexes, possibly formed HNO along with the aroyl radical (by analogy with the INH complex, Scheme 3) might quench the latter thus shortening its half-life time and preventing its detection by EPR. However, the process $HNO + ArC^{\bullet}=O \rightarrow NO^{\bullet} + PyzCHO$, would yield an aldehyde, which was not evidenced by ^1H NMR spectroscopy. Moreover, the benzile-like product of the radical coupling process $2\ ArCO^{\bullet} \rightarrow ArC(O)–C(O)Ar$ also failed to be isolated and even detected.

Another possibility is thus that, in the hydroxamic series, the carboxylic acid does not arise from an aroyl radical, but from another intermediate instead. This intermediate could be the undissociated aroyl-nitroso compound, generated upon an oxidation step, which could undergo a rapid heterolytic cleavage by the surrounding water molecules (Scheme 6), releasing HNO without any radical species, as previously suggested to occur from other hydroxamic acids [38, 39].

Inhibitory activity against *Mtb*

The antimycobacterial activity of the ligand **2** and complex **3** was investigated against the *Mtb* H37Rv reference strain, using INH as positive reference compound. The ligand **5** and the complex **6** were also introduced in these biological assays for comparison purposes. In this anti-mycobacterial assay, resazurin dye was employed to measure the lowest concentration of the tested compounds that could prevent any color change, which indicates a disruption of the growth. Those values were reported as MIC (minimum inhibitory concentration), which, for compounds **2** and **3**, **5** and **6** were, respectively, 100 and > 100 μg/mL, and for INH was 0.39 μg/mL. These results indicate that even at considerably high concentrations, there is no measurable inhibition of *Mtb* growth under these experimental conditions. However, putative activity against of *Mtb* strains within activated macrophage, or even in the non-replicating *Mtb* state, deserves further investigations.

Vasodilatory and antihypertensive activity

Aiming to test the hypothesis that metal complex **3** or $\mathbf{3}H^+$ can release HNO/NO, vasodilation assays were performed. Again, the ligand **2** and **5** and the complex **6** were also tested for comparison. The NO species is indeed known to induce vasodilation of blood vessels, and NO carrier molecules, such as sodium nitroprusside (SNP, $Na_2[Fe^{II}(CN)_5(NO)]$), have an important therapeutic effect for hypertensive crises [40]. At the same time, HNO, the reduced and protonated form of NO·, has also been reported to exhibit vasodilation activity, and shares many similar biological features of NO· [38, 39]. The structural analogy of the complexes **3** and **6** with SNP was thus a natural argument for such investigations, along with our further experimental evidences for HNO production (Fig. 4). Indeed, an assay carried out side-by-side with SNP and complexes **3** and **6** showed an interesting profile of vasodilation. While the free ligands **2** and **5** exhibited an expressively higher EC_{50} value for vasodilation activity at 19 μM, the metal complex **3** had an EC_{50} value of 250 nM only, a remarkable enhancement of 76-fold. Additionally, EC_{50} values for the complex **3** is 19-fold higher than SNP as measured side-by-side ($EC_{50} = 13$ nM). The complex **6** exhibits lower EC_{50} (64 nM) than **3** and SNP is only a fivefold more potent than **6**. The beneficial role of the iron complex moiety for vasodilation properties can be promptly noted by comparing the EC_{50} values of **2** and **3** and also **5** and **6** (Fig. 5). The concentration–response curve for the vasodilation experiments showed that the complex **3** as compared to SNP has the same efficacy and similar potency, which is a priori promising for the design of an alternative drug. Although SNP has several indications in cardiology such as heart failure, angina, after cardiac surgeries, hypertensive crisis, hypertensive encephalopathy, cardiogenic pulmonary oedema, it also has several contraindications and limitations such as liver toxicity, reflex tachycardia, and electrocardiographic alterations.

Although the water-soluble complexes **3** and **6**, able to release HNO/NO, are less potent than SNP, this can be an advantage because SNP, releasing NO rapidly, can cause major drops in blood pressure, thus requiring a careful control through titration.

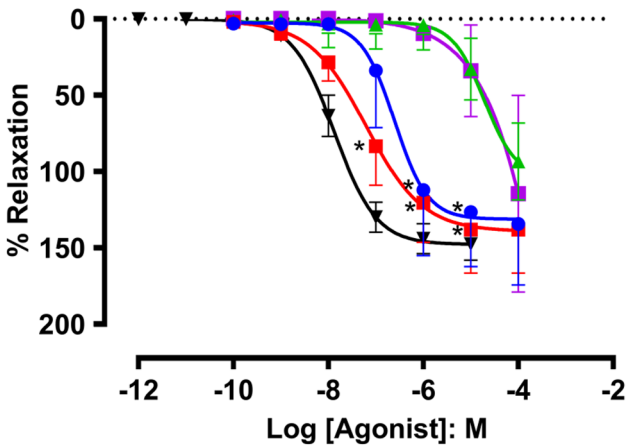

Fig. 5 Relaxation effects on aortic rings pre-contracted with 0.1 μM phenylephrine: $[Fe(CN)_5(\text{pyrazine-2-hydroxamic acid})]^{3-}$ (**3**) (blue), $Fe(CN)_5(\text{pyridine-4-hydroxamic acid})]^{3-}$ (**6**) (red), pyrazine-2-hydroxamic acid (**2**) (green), isonicotinoic hydroxamic acid (**5**) (purple) and SNP (black). $^*p < 0.05$ vs. pyrazine-2-hydroxamic acid and isonicotinoic hydroxamic acid. The IC_{50} and respective 95% confidence interval were calculated only for **3** (250 nM, 91–690 nM) and **6** (64 nM, 25–160 nM)

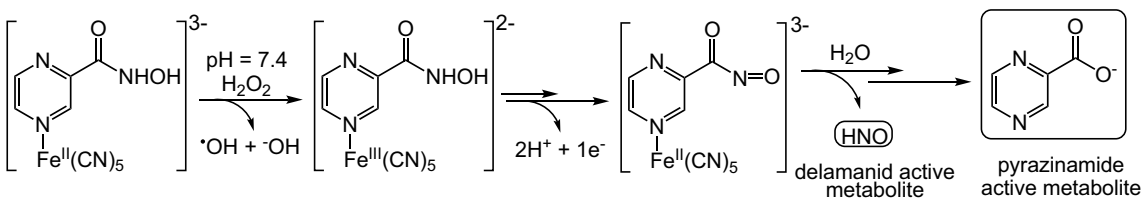

Scheme 6 Proposed outcome of the chemical oxidation of complex **3** under its trianionic form $\mathbf{3}H^+$ with H_2O_2

The complexes **3** and **6** can be all the more interesting since their efficacy (maximum relaxation effect) is quite similar to that of SNP. We should also point out that, in contrast to SNP, whose release of NO also promotes cyanide dissociation, the process is greatly reduced for new pentacyanoferrate complexes. Actually, a quick comparison of the lethal dose of SNP and the pentacyanoferrate(II)-INH complex (IQG607) illustrates this topic (mouse orally administered with SNP and IQG607 LD50 = 61 mg/kg and 2970 mg/kg, respectively), where SNP is over 48-fold more lethal [14, 41]. It is also noteworthy that those values correspond to oral dosages, but considering that pentacyanoferrate(II) complexes are particularly instable in acidic conditions—occurring in the rats' stomach— leading to decomposition and cyanide release—the real activity level might be even higher with other administration routes.

All these results indicate that the complex **3** or **6** might be a suitable model for designing alternative anti-hypertensive drugs. Modulation of the electronic effects on the metal center and changes on the aromatic hydroxamic ligand moiety might lead to more efficient tuning of their properties to achieve adjustable HNO/NO release. For instance, the compound **6**, which exhibited the lower EC_{50} (64 nM), was demonstrated to decrease blood pressure more efficiently in hypertensive rats (SHR) than its normotensive matched controls (Fig. 6). The doses of 1, 5, and 10 mg/kg promoted a drop in blood pressure equivalent to 45.6 ± 1.9%, 62.1 ± 2.5% and 65.1 ± 3.1% in SHR rats and 30.8 ± 2.3, 50.9 ± 4.2 and 53.3 ± 3.3 in normotensive rats, respectively. This compound did also increase cardiac output significantly, probably secondary to a decreased afterload and increased coronary flow.

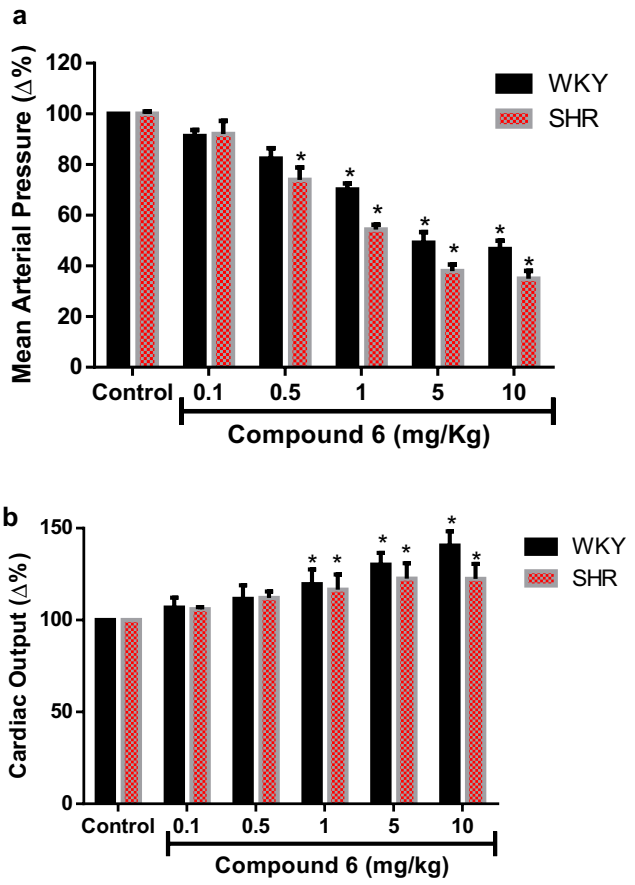

Fig. 6 Antihypertensive (**a**) and increased cardiac output (b) induced by compound **6** in normotensive (WKY) rats or spontaneously hypertensive rats (SHR). *$p < 0.05$ vs. control (administration of the vehicle)

Conclusion

The proposed strategy for metal-mediated oxidative activation of hybrid prodrugs, has been investigated for the anti-*Mtb* metabolites of pyrazinamide and delamanid in the hydroxamic hybrid series. The results unveil biological prospects of Fe(II) coordination complexes in pharmacophore design, while spanning a bridge between far-related medicinal challenges, from anti-bacterial to vasodilation effects. The complex **3** in the presence of H_2O_2 gave direct and indirect evidences for the release of pyrazinoic acid and HNO, respective active metabolites of pyrazinamide and delamanid. Although this complex did not exhibit anti-*Mtb* activity on actively growing non-resistant strains, further investigations may be warranted employing either/both single-condition whole-cell models (e.g., fatty acid carbon sources, hypoxia, low pH, biofilm, and carbon starvation) or/and multistress condition whole-cell models that try to recapitulate nonreplicating persistent bacilli, upon which pyrazinamide is active. Furthermore, promising advances have been established for antihypertensive therapy, where the hydroxamic complexes **3** and **6** have been shown to be globally as active as the SNP drug, with a more regular action and significantly lower toxicity. Additionally, comparison of vasodilation properties of **3** and **6** with those of **2** and **5** respectively, clearly show that the pentacyanoferrate moiety plays a beneficial role in the efficiency of the release of HNO from hydroxamic acids. Investigation of the expected longer duration of vasodilatory action of **3** and **6** will be performed in due course by systematic pharmacodynamic (PD) studies.

Acknowledgements The authors would also like to acknowledge financial support given by CNPq/FAPERGS/CAPES/BNDES to the National Institute of Science and Technology on Tuberculosis (INCT-TB), Brazil [grant numbers: 421703-2017-2/17-1265-8/14.2.0914.1; LGFLopes: CNPq 303355/2018-2; EHSS: CNPq 308383/2018-4, Universal 403866/2016-2) and COFECUB Project n° Ph-C 883/17. This study was financed in part by the Coordenação de Aperfeiçoamento de Pessoal de Nível Superior—Brasil (CAPES)—Finance Code 001.

Additionally, we are also in debt with Iury A. Paz, Renata Oliveira Santiago and Ariana Gomes da Silva for their assistance on the preliminary biological studies.

Compliance with ethical standards

Conflict of interest The authors declare have no conflict of interest.

Ethical approval All procedures were performed according to the ethics committee of State University of Ceará number 2897836/15.

References

1. Health World Organization annual report https://www.who.int/tb/publications/global_report/en/ Accessed 30 April 2020.
2. Ryan NJ, Lo JH (2014) Delamanid: first global approval. Drugs 74:1041–1045
3. Rustomjee R, Zumla A (2015) Delamanid expanded access novel treatment of drug resistant tuberculosis. Infect Drug Resist 8:359–366
4. Matsumoto M, Hashizume H, Tomishige T, Kawasaki M, Tsubouchi H, Sasaki H, Shimokawa Y, Komatsu M (2006) OPC-67683, a nitro-dihydro-imidazooxazole derivative with promising action against tuberculosis in vitro and in mice. PloS Med 3:e466
5. Singh R, Manjunatha U, Boshoff HIM, Ha YH et al (2008) PA-824 Kills Nonreplicating Mycobacterium tuberculosis by Intracellular NO Release. Science 322:1392–1395
6. Laborde J, Deraeve C, Bernardes-Génisson V (2017) Update of antitubercular prodrugs from a molecular perspective: mechanism of action, bioactivation pathways and associated resistance. ChemMedChem 12:1657–1676
7. Lopez BE, Shinnyashiki M, Han TH, Fukuto JM (2007) Antioxidant actions of nitroxyl (HNO). Free Radical Biol Med 42:482–491
8. Norris AJ, Sartippour MR, Lu M, Park T, Rao JY, Jackson MI, Fukuto JM, Brooks MN (2008) Nitroxyl inhibits breast tumor growth and angiogenesis. Int J Cancer 122:1905–1910
9. Nelli S, McIntosh L, Martin W (2001) Role of copper ions and cytochrome P450 in the vasodilator actions of the nytroxyl anion generator, Angeli's salt, on rat aorta. Eur J Pharmacol 412:281–289
10. Sousa EHS, Basso LA, Santos DS, Diógenes ICN, Longhinotti E, Lopes LGF, Moreira IS (2012) Isoniazid metal complex reactivity and insights for a novel anti-tuberculosis drug design. J Biol Inorg Chem 17:275–283
11. Basso LA, Schneider CZ, Santos AJAB, Santos AA Jr, Campos MM, Souto AA, Santos DS (2010) An inorganic complex that inhibits mycobacterium tuberculosis enoyl reductase as a prototype of a new class of chemotherapeutic agents to treat tuberculosis. J Braz Chem Soc 21:1384–1389
12. Sousa EHS, Pontes DL, Diogènes ICN, Lopes LGF, Oliveira JS, Basso LA, Santos DS, Moreira IS (2005) Electron transfer kinetics and mechanistic study of the thionicotinamide coordinated to the pentacyanoferrate(III)/(II) complexes: a model system for the in vitro activation of thioamides anti-tuberculosis drugs. J Inorg Biochem 99:368–375
13. Abbadi BL, Villela AD, Rodrigues-Junior VS, Subtil FT, Dalberto PF, Pinheiro APS, Santos DS, Machado P, Basso LA, Bizarro CV (2018) Revisiting activation of and mechanism of resistance to compound IQG-607 in *Mycobacterium tuberculosis*. Antimicrob Agents Chemother 62:e2222–e2317
14. Abbadi BL, Rodrigues-Junior VS, Dadda AS, Pissinate K, Villela AD, Campos MM, Lopes LGF, Bizarro CV, Machado P, Sousa EHS, Basso LA (2018) Is IQG-607 a potential metallodrug or metallopro-drug with a defined molecular target in Mycobacterium tuberculosis? Front Microbiol 9:880
15. Zhang Y, Mitchison D (2003) The curious characteristics of pyrazinamide: a review. Int J Tuberc Lung Dis 7:6–21
16. Vandal OH, Nathan CF, Ehrt S (2009) Acid resistance in *Mycobacterium tuberculosis*. J Bacteriol 191:4714–4721
17. Zhang Y, Mitchison D, Shi W, Zhang W (**2014**) Mechanisms of pyrazinamide action and resistance. Microbiol. Spectr. 2: MGM2-0023-2013
18. Njire M, Tan Y, Mugweru J, Wang C, Guo J, Yew W, Tan S, Zhang T (2016) Pyrazinamide resistance in *Mycobacterium tuberculosis*: review and update. Adv Med Sci 61:63–71
19. Stehr M, Elamin AA, Singh M (2015) Pyrazinamide: the importance of uncovering the mechanisms of action in mycobacteria. Expert Rev Anti Infect Ther 13:593–603
20. Pires BM, Jannuzzi SAV, Formiga ALB, Bonacin JA (2014) Prussian blue films produced by pentacyanidoferrate(II) and their application as active electrochemical layers. Eur J Inorg Chem 2014:5812–5819
21. Becke AD (1993) Density-functional thermochemistry. III. The role of exact exchange. J Chem Phys 98:5648–5652
22. Lee C, Yang W, Parr RG (1988) Development of the Colle-Salvetti correlation-energy formula into a functional of the electron density. Phys Rev B 37:785–789
23. Stephens PJ, Devlin FJ, Chabalowski CF, Frisch MJ (1994) Ab Initio calculation of vibrational absorption and circular dichroism spectra using density functional force fields. J Phys Chem 98:11623–11627
24. Frisch MJ, Trucks GW, Schlegel HB, Scuseria GE, Robb MA, Cheeseman JR, Scalmani G, Barone V, Mennucci B, Petersson GA, Nakatsuji H, Caricato M, Li X, Hratchian HP, Izmaylov AF, Bloino J, Zheng G, Sonnenberg JL, Hada M, Ehara M, Toyota K, Fukuda R, Hasegawa J, Ishida M, Nakajima T, Honda Y, Kitao O, Nakai H, Vreven T, Montgomery JA Jr, Peralta JE, Ogliaro F, Bearpark M, Heyd JJ, Brothers E, Kudin KN, Staroverov VN, Kobayashi R, Normand J, Raghavachari K, Rendell A, Burant JC, Iyengar SS, Tomasi J, Cossi M, Rega N, Millam JM, Klene M, Knox JE, Cross JB, Bakken V, Adamo C, Jaramillo J, Gomperts R, Stratmann RE, Yazyev O, Austin AJ, Cammi R, Pomelli C, Ochterski JW, Martin RL, Morokuma K, Zakrzewski VG, Voth GA, Salvador P, Dannenberg JJ, Dapprich S, Daniels AD, Farkas O, Foresman JB, Ortiz JV, Cioslowski J, Fox DJ (2013) Gaussian 09, Revision D.01. Gaussian Inc, Wallingford
25. Tomasi J, Mennucci B, Cammi R (2005) Quantum mechanical continuum solvation models. Chem Rev 105:2999–3093
26. O'Boyle NM, Tenderholt AL, Langner KM (2008) Cclib: a library for package-independent computational chemistry algorithms. J Comput Chem 29:839–845
27. Giacobbo BC, Pissinate K, Rodrigues-Junior V, Villela AD, Grams ES, Abbadi BL, Subtil FT, Sperotto N, Trindade RV, Back DF, Campos MM, Basso LA, Machado P, Santos DS (2017) New insights into the SAR and drug combination synergy of 2-(quinolin-4-yloxy)acetamides against *Mycobacterium tuberculosis*. Eur J Med Chem 126:491–501
28. Kushner S, Dalalian H, Sanjurjo JL, Bach FL Jr, Safir SR, Smith VK Jr, Williams JH (1952) Experimental chemotherapy of tuberculosis. II. The Synthesis of pyrazinamides and related compounds. J Am Chem Soc 74:3617–3621
29. Zhang YY, Gao W-X, Lin Y-J, Mi L-W, Jin G-X (2017) Syntheses, structures, and solution studies of multicomponent macrocycles and cages based on versatile ligands. Chem Eur J 23:11133–11140
30. Hackley BE Jr, Plafinger R, Stolberg M, Wagner-Jauregg T (1955) Accelaration of the hydrolysis of organic fluoro-phosphates and

fluorophosphonates with hydroxamic acids. J Am Chem Soc 77:3651–3653
31. Laborde J, Deraeve C, Vieira FGM, Sournia-Saquet A, Rechignat L, Villela AD, Abbadi BL, Macchi FS, Pissinate K, Lopes LGF, Sousa EHS, Pratviel G, Bernardes-Génisson V (2018) Synthesis and mechanistic investigation of iron(II) complexes of isoniazid and derivatives as a redox-mediated activation strategy for anti-tuberculosis therapy. J Inorg Biochem 179:71–81
32. Grandjean F, Samain L, Long GJ (2016) Characterization and utilization of Prussian blue and its pigments. Dalton Trans 45:18018–18044
33. Carvalho EM, Rechignat L, Sousa EHS, Lopes LGF, Chauvin R, Bernardes-Génisson V (2020) Mechanistic insights into the in vitro metal-promoted oxidation of (di)azine hydroxamic acids: evidence of HNO release and N, O-di(di)azinoyl hydroxylamine intermediate. New J Chem 44:11965–11973
34. Samuni U, Samuni Y, Goldstein S (2010) On the distinction between nitroxyl and nitric oxide using nitronyl nitroxides. J Am Chem Soc 132:8428–8432
35. Bobko AA, Ivanov A, Khramtsov VV (2013) Discriminative EPR detection of NO and HNO by encapsulated nitronyl nitroxides. Free Radic Res 47:74–81
36. Bobko AA, Khramtsov VV (2015) Redox properties of the nitronyl nitroxide antioxidants studied via their reactions with nitroxyl and ferrocyanide. Free Radic Res 49:919–926
37. Sousa EHS, Vieira FGM, Butler JS, Basso LA, Santiago DS, Santiago DS, Diógenes ICN, Lopes LGF, Sadler PJ (2014) $[Fe(CN)_5(isoniazid)]^{3-}$: an iron isoniazid complex with redox behavior implicated in tuberculosis therapy. J Inorg Biochem 140:236–244
38. Maimon E, Lemer A, Samuni A, Goldstein S (2018) Direct observation of acyl nitroso compounds in aqueous solution and the kinetics of their reactions with amines, thiols, and hydroxamic acids. J Phys Chem A 122:7006–7013
39. Maimon E, Lemer A, Samuni A, Goldstein S (2018) Nitrogen dioxide reaction with nitroxide radical derived from hydroxamic acids: the intermediacy of acyl nitroso and nitroxyl (HNO). J Phys Chem A 122:3747–3753
40. Silva Filho PM, Paz IA, Nascimento NRF, Santos CF, Araújo VR, Aquino CP, Ribeiro TS, Vasconcelos IF, Lopes LGF, Sousa EHS, Longhinotti E (2019) Incorporation of nitroprusside on silica nanoparticles—a strategy for safer use of this no donor in therapy. Mol Pharm. 16:2912–2921
41. RTECS—Register of toxic effects of chemical substances. https://www.cdc.gov/niosh/docs/97-119/default.html. Accessed 30 Apr 2020

Affiliations

Edinilton Muniz Carvalho[1,2,3] · Tercio de Freitas Paulo[1,2,3] · Alix Sournia Saquet[1] · Bruno Lopes Abbadi[4,5] · Fernanda Souza Macchi[4,5] · Cristiano Valim Bizarro[4,5] · Rafael de Morais Campos[6] · Talles Luann Abrantes Ferreira[6] · Nilberto Robson Falcão do Nascimento[6] · Luiz Gonzaga França Lopes[3,5] · Remi Chauvin[1,2] · Eduardo Henrique Silva Sousa[3,5] · Vania Bernardes-Génisson[1,2]

1 CNRS, Laboratoire de Chimie de Coordination, LCC, UPR 8241, 205 Route de Narbonne, BP 44099, 31077 Cedex 4 Toulouse, France

2 Université de Toulouse, Université Paul Sabatier, UPS, 118 Route de Narbonne, 31062 Cedex 9, Toulouse, France

3 Grupo de Bioinorgânica, Departamento de Química Orgânica E Inorgânica, Universidade Federal Do Ceará, Campus Pici, Fortaleza, CE 60455-760, Brazil

4 Centro de Pesquisas Em Biologia Molecular E Funcional (CPBMF), Pontifícia Universidade Católica Do Rio Grande Do Sul (PUCRS), Porto Alegre, Brazil

5 Instituto Nacional de Ciência E Tecnologia Em Tuberculose (INCT-TB), Porto Alegre, Brazil

6 Laboratório de Farmacologia Cardiovascular E Renal, Universidade Estadual Do Ceará, Campus do Itaperi, Fortaleza, CEP 60714-903, Brazil